



RESEARCH ARTICLE | AUGUST 01 2016

The effects of nanoparticles and organic additives with controlled dispersion on dielectric properties of polymers: Charge trapping and impact excitation

Yanhui Huang (黄彦辉); Ke Wu; Michael Bell; Andrew Oakes ; Tyree Ratcliff; Nicholas A. Lanzillo; Curt Breneman; Brian C. Benicewicz; Linda S. Schadler 



J. Appl. Phys. 120, 055102 (2016)

<https://doi.org/10.1063/1.4959771>



Articles You May Be Interested In

Laser direct write printing of sensitive and robust light emitting organic molecules

Appl. Phys. Lett. (March 2009)

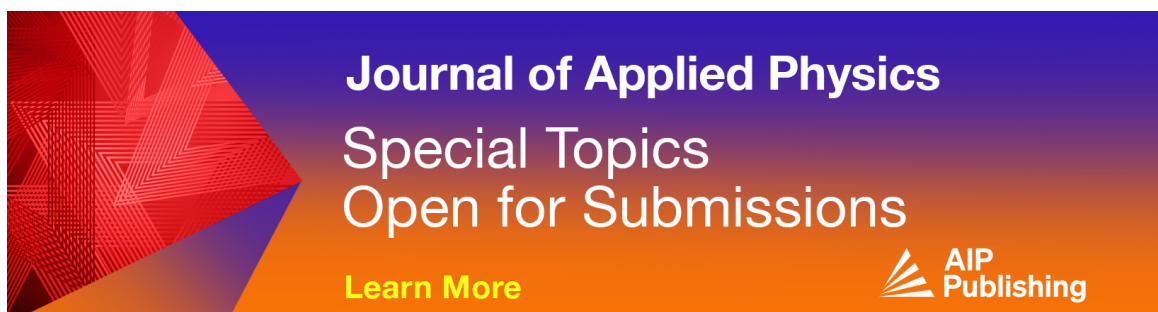
On the nature of high field charge transport in reinforced silicone dielectrics: Experiment and simulation

J. Appl. Phys. (August 2016)

Predicting the breakdown strength and lifetime of nanocomposites using a multi-scale modeling approach

J. Appl. Phys. (August 2017)

20 June 2025 16:38:37



Journal of Applied Physics

Special Topics

Open for Submissions

[Learn More](#)



The effects of nanoparticles and organic additives with controlled dispersion on dielectric properties of polymers: Charge trapping and impact excitation

Yanhui Huang (黄彦辉),^{1,a)} Ke Wu,² Michael Bell,³ Andrew Oakes,³ Tyree Ratcliff,² Nicholas A. Lanzillo,² Curt Breneman,² Brian C. Benicewicz,³ and Linda S. Schadler¹

¹Department of Material Science and Engineering, Rensselaer Polytechnic Institute, Troy, New York 12180, USA

²Department of Chemistry and Chemical Biology, Rensselaer Polytechnic Institute, Troy, New York 12180, USA

³Department of Chemistry and Biochemistry, University of South Carolina, Columbia, South Carolina 29208, USA

(Received 20 January 2016; accepted 12 July 2016; published online 1 August 2016)

This work presents a comprehensive investigation into the effects of nanoparticles and organic additives on the dielectric properties of insulating polymers using reinforced silicone rubber as a model system. TiO₂ and ZrO₂ nanoparticles ($d = 5$ nm) were well dispersed into the polymer via a bimodal surface modification approach. Organic molecules with the potential of voltage stabilization were further grafted to the nanoparticle to ensure their dispersion. These extrinsic species were found to provide deep traps for charge carriers and exhibited effective charge trapping properties at a rather small concentration ($\sim 10^{17}$ cm⁻³). The charge trapping is found to have the most significant effect on breakdown strength when the electrical stressing time is long enough that most charges are trapped in the deep states. To establish a quantitative correlation between the trap depth and the molecular properties, the electron affinity and ionization energy of each species were calculated by an *ab initio* method and were compared with the experimentally measured values. The correlation however remains elusive and is possibly complicated by the field effect and the electronic interactions between different species that are not considered in this computation. At high field, a super-linear increase of current density was observed for TiO₂ filled composites and is likely caused by impact excitation due to the low excitation energy of TiO₂ compared to ZrO₂. It is reasoned that the hot charge carriers with energies greater than the excitation energy of TiO₂ may excite an electron-hole pair upon collision with the NP, which later will be dissociated and contribute to free charge carriers. This mechanism can enhance the energy dissipation and may account for the retarded electrical degradation and breakdown of TiO₂ composites. *Published by AIP Publishing.* [<http://dx.doi.org/10.1063/1.4959771>]

I. INTRODUCTION

Introducing nanoparticles (NPs) or organic molecules with voltage stabilizing properties (e.g. anthracene) have been shown to improve polymer dielectric properties including voltage endurance, breakdown strength, and volume resistivity.¹⁻⁴ But there is limited consensus on the mechanism leading to these improvements, and some results are even conflicting.^{1,5} Our earlier studies showed that the localized state (trap state) in polymer dielectrics is of crucial importance to the charge transport under high field and is closely associated with the macroscopic dielectric properties, including charge injection, space charge distribution, and transport mobilities.⁶ Therefore, it is expected that filling polymers with these extrinsic species will introduce new electronic states and alter the spatial and energy distribution of the localized states in the material, which may account for the changes in dielectric properties of nanodielectrics.

In this work, SiO₂ reinforced silicone rubber was used as a model system to comprehensively study the electronic effects of NPs and voltage stabilizing organic molecules³ on the

dielectric properties of insulating polymers. Silicone rubber is selected because of its easy processability for high quality films, narrow breakdown strength dispersion, and well-developed chemistry for NP dispersion control. Also, silicone has not been extensively studied as polyethylene and epoxy and therefore can serve as a complementary example to examine the universality of the effects of nanofillers in dielectric polymers. Thanks to its entire compatibility with the polymer and low cost, SiO₂ NPs are normally added heavily to silicone as reinforcing fillers to improve the mechanical and electrical properties. Our previous work has shown that the SiO₂ reinforced silicone exhibits a retarded space charge transport compared to the unfilled silicone. But as a large portion of the material is SiO₂ NPs (40 wt. %), it is unclear whether the reduced mobility is caused by morphological changes to the polymer or by deep traps on SiO₂.⁶ Since SiO₂ NPs are homogeneously dispersed in the polymer (the material is entirely transparent), in this study, we treat the reinforced silicone as a homogeneous matrix and primarily study the effect of a small amount (~ 0.5 vol. %) of additionally added NPs.

It has been shown that the dispersion and morphology of NPs and molecular additives can be critical to the dielectric properties.^{2,7} Dispersion, however, is difficult to control and

^{a)}Author to whom correspondence should be addressed. Electronic mail: huangy12@rpi.edu

tends to vary significantly across different systems,⁸ rendering it difficult to directly compare results. In this work, we specifically controlled the geometrical distribution of TiO₂ and ZrO₂ NPs by employing a bimodal surface modification method: two populations of polymer brushes with different lengths were grafted to the NP to enhance the dispersion in the matrix polymer.^{9–12} In addition, organic molecules with potential voltage stabilizing properties were grafted to the bimodally modified NP to ensure their dispersion as well. The charge trapping effect was thoroughly investigated and confirmed in multiple measurements. To correlate the trap depth with the molecular properties of NP and organic molecules, the electron affinity (EA) and ionization energy (IE) were computed by density functional theory (DFT) and compared with the experimentally measured trap depth. The super-linear increase of current density at high field and the increased AC breakdown strength in TiO₂ filled composites suggest an impact excitation mechanism to effectively dissipate the energy of hot carriers.

II. EXPERIMENTAL

A. NP synthesis and surface modification

The synthesis of TiO₂ and ZrO₂ NPs and the surface modification with two populations of polydimethylsiloxane (PDMS) brushes was reported in our earlier publications.^{9,10,13} The NPs are highly crystalline (anatase for TiO₂ and cubic for ZrO₂) and are mono-disperse with a diameter of 5 ± 1 nm.¹⁴ PDMS of 36k molecular weight (MW) with a graft density of 0.01 ch/nm² and PDMS of 10k MW with a graft density of 0.1 ch/nm² were sequentially grafted to the NP through a phosphonic acid end group. The graft density was confirmed by thermogravimetric analysis (TGA).

The PDMS grafted NPs were further grafted with a layer of small organic molecules that are potential voltage stabilizers. The molecules were attached to the NP through either a carboxylic or phosphonic acid end group. In a typical synthesis, NPs were combined with molecules in a tetrahydrofuran (THF) solution under an ice bath, and the mixture was then allowed to warm up to room temperature and stirred overnight. NPs were recovered by precipitation in methanol followed by centrifuging, and the ungrafted molecules were washed away with methanol in the supernatant. NPs were then re-dispersed in THF. This procedure was repeated three times to ensure that most ungrafted molecules were removed. The graft density was around 0.3 ch/nm² and was measured by UV-Vis spectroscopy by comparing the light absorption of the grafted NP solution with the calibrated absorption curve of free molecules.¹⁵

B. Small organic molecules as potential voltage stabilizers

Different molecules including 9-anthracenemethylphosphonic acid (An), 10-bromo-9-methyl anthracene phosphonic acid (AnBr), 1-pyrenecarboxylic acid (Py), 3-[N-(7'-Nitrobenz-2'-oxa-1',3'-diazol-4'-yl)amino]propanoic acid (NBD), and 6-[Fluorescein-5(6)-carboxamido]hexanoic acid (FCHA) were used (Fig. 1). NBD and FCHA are dye molecules with a small

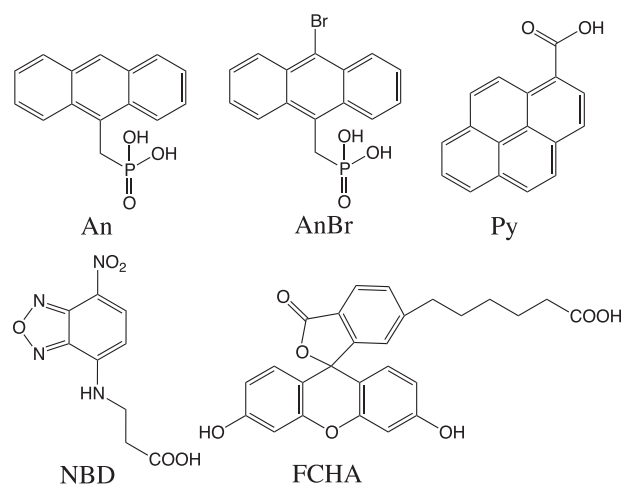


FIG. 1. The chemical structures of the small molecules used as potential voltage stabilizers.

band gap and can serve as potential charge trapping centers. FCHA and Py were purchased from Sigma-Aldrich. The synthesis of NBD can be found elsewhere.¹⁴ The synthesis of An and AnBr are described as follows.

9-Anthracenemethanol (2 g) was dissolved into 40 ml of toluene before cooling to 0°C. Phosphorous tribromide (3.12 g) was added dropwise. The solution was allowed to warm to room temperature and stirred overnight. The reaction was washed with one portion 2 M Na₂CO₃ and two portions of water. After isolating the organic portion, drying, and removing solvent, 9-(bromomethyl) anthracene was obtained as a yellow solid. Next 9-(bromomethyl)anthracene (2.22 g) and triethyl phosphate (5 g) were refluxed overnight under nitrogen. The product, diethyl 9-anthracene methylphosphate (2.41 g) was precipitated from solution at 0°C. The obtained 9-anthracenemethylphosphonate was converted to the free phosphonic acid derivative using excess bromotrimethylsilane in dichloromethane, yielding 9-anthracenemethylphosphonic acid (2 g) as the final product. The brominated version of anthracene was synthesized by refluxing 9-anthracenemethanol (2 g) and an equimolar amount of bromine in carbon tetrachloride (100 ml) for 2 h. The reaction was cooled to room temperature and washed with three portions of water. The organic phase was isolated and solvent was removed. The solid product 10-bromo, 9-anthracenemethanol was then recrystallized 3× in toluene giving a final yield of 1.2 g. The hydroxy group was converted to phosphonic acid in the same manner as described above.

C. Sample preparation

Silicone rubber Sylgard[®] 184 from Dow Corning was used as the polymer matrix, which is reinforced with 40 wt. % fumed SiO₂. The resin was dissolved in THF to mix with NPs and the solvent was then removed by vacuum evaporation. The hardener was added at a 10:1 weight ratio before shear mixing at 3500 rpm for 1 min. The resin was cast in a flat aluminum dish and cured at 110°C under vacuum for 1.5 h. The cured samples were stored in a desiccator and conditioned at 70°C under vacuum overnight before dielectric test. Unless otherwise indicated, the sample had a NP

loading of 2 wt. % with a thickness of $380 \pm 30 \mu\text{m}$ and a diameter of 3 cm. In the following discussion, the sample name is abbreviated using the form of “NP-molecule.”

D. Characterizations

The NP dispersion was examined using transmission electron microscopy (TEM) by microtoming the sample at -140°C with a thickness of 80 nm. The space charge distribution was measured using a pulsed-electro-acoustic (PEA) method. The details of the PEA measurements can be found in our previous paper.⁶ In the DC conductivity measurement, a $50 \pm 5 \mu\text{m}$ thin film was spin-coated on an aluminum disk, and the sample was subjected to a stepwise increase in field of 5 MV/m with a 10 min stabilization time at each voltage up to breakdown. A flat guarded electrode of 20 mm diameter was used. The quasi-steady state current and the final breakdown voltage were recorded. For AC breakdown, a $400 \pm 30 \mu\text{m}$ film was used, and the top spherical electrode is made of stainless steel with a diameter of 5 mm, and the exact thickness at each test point is measured before testing. The ground electrode is the Al dish on which the sample is cured. The voltage was ramped by 500 V/s. Dielectric spectroscopy was measured using a Novocontrol Alpha analyzer with a voltage of 1 V. For the photoluminescence measurement, the film was placed perpendicular to the excitation beam from a Xenon source and the detector was placed 90° to the beam. The same sample was measured by UV-Vis spectroscopy to determine the light absorption.

E. DFT calculations

Quantum computation of the electron affinity (EA) and ionization energy (IE) of isolated molecules was performed using Gaussian09.¹⁶ Cation, anion, and neutral molecules were first prepared using the PM3 method. Then, the first stage of optimization was performed by HF/6-31 G*, and the resulting geometry and orbitals were used as the input for the second stage using B3lyp/6-31+G*.¹⁷⁻¹⁹ B3lyp shows good performance on the computation on radicals and with only slight spin contamination. The zero-point-energy (ZPE) was also calculated, and a correction coefficient 0.75 was used. The optimized structure was used to calculate the electronic energy using B3lyp/6-311++G**. The final energy was calculated as the sum of the electronic energy and the corrected ZPE.

III. CHARGE TRAPPING

A. Theoretical considerations

1. Thermodynamics

We showed in our previous paper that the energy and spatial distribution of localized states in a polymer are critical to the charge transport properties.⁶ When NPs are introduced into the polymer matrix, the extrinsic electronic states on the NP will act as additional hopping sites for charge carriers. Time resolved photo-excitation spectroscopy shows that once the carrier is injected into a crystalline NP, it will quickly delocalize inside the NP and relax to the band

bottom within a time scale of 100 fs,²⁰ which is much shorter than the typical trapping time in polymers. In this case, it is only necessary to consider the effect of the lowest electronic states in the NP, as it is these states that eventually determine the trap depth. Given the low carrier concentration and the large columbic repulsion force when two homocharges are confined in one NP, we would expect each NP to trap one carrier at a time. Based on these considerations, each NP can be treated as a single trap site characterized by its lowest energy.

Some small conjugated organic molecules, known as “voltage stabilizers” can also offer deep traps and are often added to polymer dielectrics.^{3,21,22} To legitimately compare the relative trap depth of different molecules, ionization energy (IE) and electron affinity (EA) are used.²¹ IE is defined as the minimum energy required to remove an electron from a molecule at ground state to vacuum while EA is the maximum energy released to accept an excess electron from vacuum to the ground state molecule. In terms of chemistry, IE and EA can be used in a similar fashion as Gibbs free energy to determine the direction of the charge transfer reaction. A smaller IE means that the molecule in its positively charged form is more stable and thus features a deeper trap for holes, while a larger EA features a deeper trap for electrons. The sign is defined to be positive for the endothermic process and negative for the exothermic one. For crystals, the equivalents are the valence band minimum (VBM) and conduction band minimum (CBM) for IE and EA, respectively. The IE and EA of an amorphous polymer are difficult to define due to the presence of localized states extending to the gap and should thus be treated as a local value instead of a global one. Ideally, the difference between IE/EA values of different species can be used as the trap depth if their vacuum levels are perfectly aligned upon contact. But in practice this is rarely the case, because electronic interactions arise when two species are brought into vicinity and this will lead to localized charge transfer or displacement at the interface and thus offset the vacuum level.^{23,24} The detailed mechanism can be complex and a unified understanding has not been achieved.²⁵ It was found that for metal/semiconductor interfaces, the offset decreases with decreasing electronic dielectric constant of the semiconductor (including wide gap insulator like SiO_2).²³ If this relation extends to molecular solids, we would expect the vacuum level offset to be less prominent for dielectric polymers since the electrons in these molecules are strongly localized and yield a small electronic dielectric constant. For NPs, the deep surface states may be present in the gap and the actual trap depth could also deviate from that of perfect crystals. Despite these complexities, we use IE and EA as a starting point to estimate the trap depth.

In the hopping transport model, the charge transfer between different states is described as a phonon-assisted tunneling process and the hopping rate can be calculated by Miller-Abraham formula²⁶

$$v_{ij} = v_0 \exp(-2\gamma R_{ij}) \times \begin{cases} \exp(-E_{ij}/kT), & E_{ij} > 0 \\ 1, & E_{ij} < 0 \end{cases} \quad (1)$$

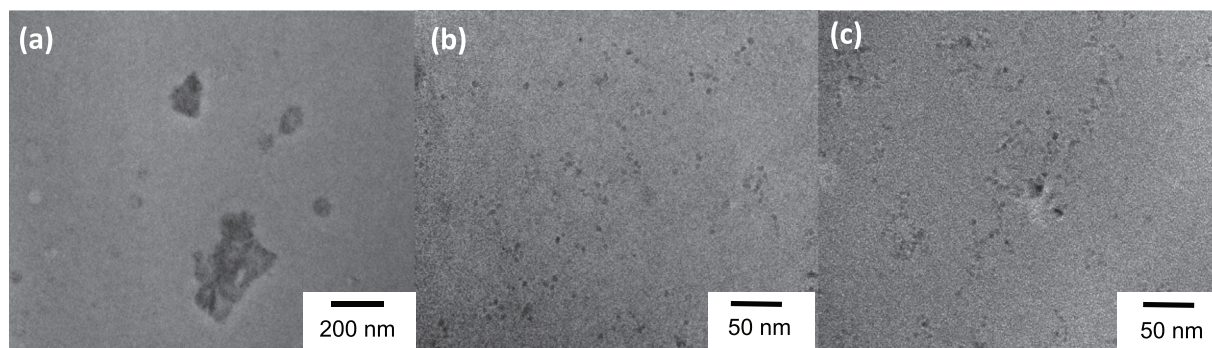


FIG. 2. The TEM images showing the dispersion state of (a) 4 wt. % as-synthesized TiO_2 and (b) 2 wt. % bimodal PDMS grafted TiO_2 and (c) TiO_2 further grafted with An. The dispersion state is similarly good for bimodal PDMS grafted ZrO_2 and when other molecules are grafted (see Fig. S2 in the supplementary material²⁹).

with v_{ij} being the hopping rate between occupied site i and unoccupied site j separated by energy E_{ij} and a distance R_{ij} , v_0 being the attempt-to-hop frequency on the order of 10^{12} Hz and γ^{-1} being the decay length of the electronic wave function. The tunneling probability decreases exponentially with the energy barrier and the distance between two states. Charges initially occupying high-density shallow states will eventually relax into deep states characterized by a sparse density. As intrinsic deep traps also prevail in polymers, effective trapping will only occur if the extrinsic states contribute appreciably to the lower end of the trap distribution.

2. Kinetics

The kinetics of charge trapping depends on the energy landscape around the NP, which is subject to the local electric field distribution and the NP/polymer interaction. As the dielectric constant of NPs is normally larger than the polymer, the curvature of the NP will bend the electric field line towards the particle and cause a local electric field concentration. Moreover, an additional long-range attractive force due to the polarization of NP will be imposed on the charge carrier and draw it to the NP, resulting in an enlarged charge capture cross-section.²⁷ The morphology of the polymer around the NP is different than that of the bulk, especially when polymer brushes are grafted onto the NP. This may result in a change of the energy landscape around the NP, but the details are unknown. The electronic interaction between NP and polymer is also critical for the charge transfer rate between two species. The importance of electronic coupling has been confirmed by studying the interfacial transfer of photoexcited electrons between TiO_2 NPs and absorbed dye molecules,²⁰ but there is a lack of studies for NP/polymer interactions.

3. Effect of dispersion

It should be noted that the underlying assumption in the abovementioned reasoning is that the extrinsic traps are well dispersed and are far away from each other, so that direct tunneling between these states is negligible. The validity of this assumption, however, can be violated if the NP loading is high or if agglomerates are formed. In such cases, direct tunneling between NPs is facilitated and a percolating path

could form, which will render the mobility highly dispersive and the overall conductivity even higher than that of the unfilled polymer. This may explain the paradox in a previous study that the found decreased mobility but increased DC conductivity when SiO_2 nanoparticles were added to cross-linked polyethylene (XLPE).⁵

The dispersion of NPs has not been well addressed and effectively controlled until recently.^{7,9} It has been shown that the dispersion of NPs can be most effectively improved by grafting a bimodal population of polymer brushes to the NP surface, with the sparsely grafted long chains enhancing the entanglement with the matrix polymer and the densely grafted short chains screening the core-core attraction between NPs.^{10,12,28} In this work, we sequentially grafted long PDMS and then short PDMS chains to the NP.¹³ As shown in Fig. 2, a good dispersion in silicone matrix is achieved, and further grafting with small organic molecules does not significantly impact the dispersion. The homogeneous dispersion yields a high transparency of the sample and can be directly verified by eyes when compared to opaque ones filled with aggregated particles. The optical images can be found in Fig. S1 in the supplementary material.²⁹

B. Effect of NP

The TiO_2 and ZrO_2 NPs were introduced into the silicone matrix as potential trapping sites for charge carriers. At a 2 wt. % loading, the particle density is $7 \times 10^{22} \text{ m}^{-3}$ with an average distance of $\sim 25 \text{ nm}$ when well dispersed. Such a large distance prevents direct tunneling between NPs and precludes percolation.

Fig. 3 shows the charge distribution evolution in the silicone matrix at a field of 10 MV/m and a bipolar charge injection and transport is observed. The more detailed discussion on charge transport properties of the silicone matrix can be found in our previous paper.⁶ Fig. 4 shows the PEA profile for bimodal PDMS grafted TiO_2 and ZrO_2 filled silicone matrix at the same nominal field. For both samples, the velocity of the electron charge packet is significantly reduced and it only moves a few micrometers into the bulk after 1 h stressing, yielding an apparent mobility of $\sim 1.5 \times 10^{-16} \text{ m}^2/\text{V s}$, about 14 times smaller than that of the silicone matrix. ZrO_2 appears to have a better hole trapping ability than TiO_2 , as the hole accumulation on the cathode only showed up at

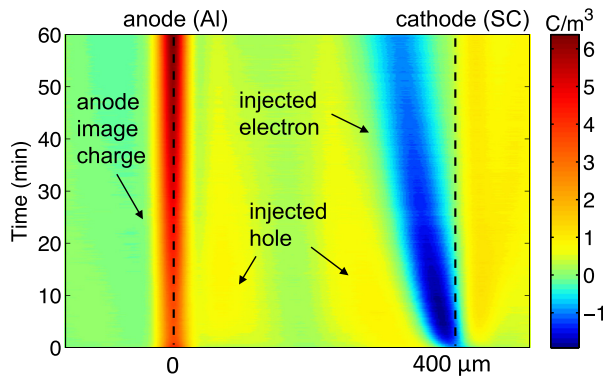


FIG. 3. The space charge profile of silicone matrix at 10 MV/m.

longer times compared to the immediate appearance in TiO_2 filled samples. But since hole transport is highly dispersive,⁶ it is difficult to directly obtain the mobility by measuring the traveling speed of the charge packet. It is possible to get around this problem by analyzing the charge decay rate of each carrier species after voltage removal, from which the trap depth can also be derived. We will discuss this in detail in Sec. III C.

The reduced electron mobility indicates that both TiO_2 and ZrO_2 can provide deep electron traps. But as shown in Table I, the CBM of TiO_2 is much lower than that of ZrO_2 , which theoretically should lead to a much deeper electron trap. TiO_2 also has a higher dielectric constant than ZrO_2 and thus should also have a higher charge trapping efficiency. Recent experiments on interfacial electron transfer from photoexcited Quinizarin to ZrO_2 NPs revealed the existence of deep surface states on ZrO_2 with an energy comparable to the CBM of TiO_2 .³⁰ So, the electron trapping on ZrO_2 may be dominated by the surface states rather than the bulk states at the CBM. The same reasoning may also apply to hole trapping, given the similar VBM of TiO_2 and ZrO_2 but different hole trapping efficiencies.

The charge trapping by TiO_2 and ZrO_2 is supported by photoluminescence spectroscopy. In this measurement, the sample is excited by a beam of light with a certain wavelength, and an electron-hole pair can be generated at the molecule by photon excitation. Trap states in the surrounding environment that are lower than the excited state of the molecule tend to suppress radiative recombination, as the excited

TABLE I. The conduction band minimum (CBM) and valence band minimum (VBM)^a of anatase TiO_2 and cubic ZrO_2 .

	TiO_2 (Ref. 31)	ZrO_2 (Ref. 32)
CBM (eV)	-5.1	-2.5
VBM (eV)	-8.3	-8.3

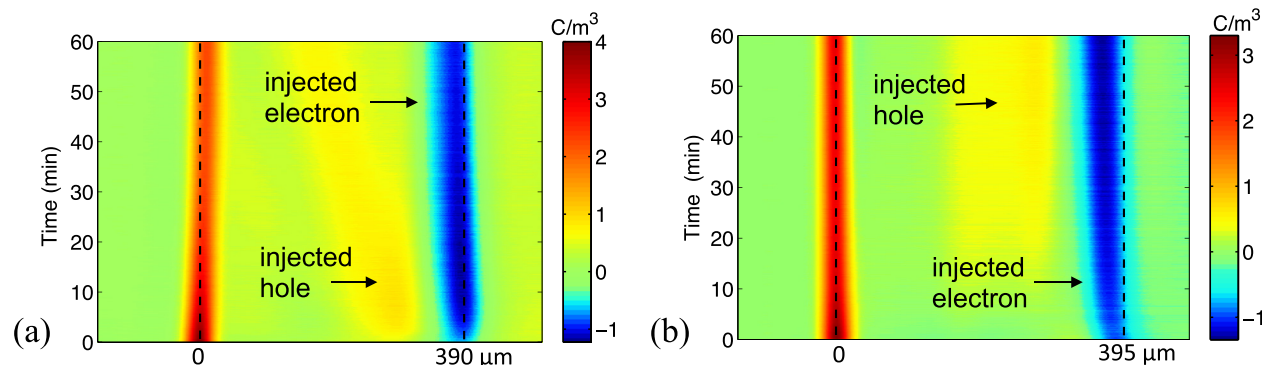
^aCBM is equivalent to EA while VBM is equivalent to -IE.

electron/hole will easily hop away and be trapped at these states. Therefore, the photoluminescence intensity will be reduced in the presence of traps. The silicone matrix contains a small amount of ethyl benzene as a chemical additive, which has light absorption between 300 to 400 nm and luminescence between 400 to 540 nm. The excitation wavelength was chosen as high as 370 nm to minimize the effect of UV absorption by TiO_2 . The measured luminescence spectra are shown in Fig. 5. It can be seen that the luminescence intensity is greatly reduced for NP filled samples though all samples have similar transparency, indicating that a majority of photoexcited carriers are trapped at neighboring NPs and direct recombination is discouraged.

C. Effect of small organic molecules

The bimodal PDMS brush grafted TiO_2 and ZrO_2 NPs were further grafted with anthracene molecules. Fig. 6 shows the space charge profile of their composites. The hole trapping ability is significantly enhanced while the electron mobility is similar to samples filled with NPs only. This result agrees with the EA and IE data calculated from DFT. Anthracene has a smaller IE of 7.2 eV compared to 8.3 eV for TiO_2 and ZrO_2 , featuring a deeper trap for holes. The EA of the anthracene molecule is only 1.4 eV, which is much smaller than the NP and should not largely impact the electron transport. The electron and hole trapping process is illustrated in Fig. 7(a).

The charge decay rate from a single trap level only depends on the remnant charge density and thus should follow an exponential behavior, $\rho = \rho_0 \exp(-t/\tau)$, where τ^{-1} quantifies the detrapping rate and ρ_0 is the initial charge density. Fig. 8 compares the charge decay rate (Fig. 8(a)) and decay profile (Figs. 8(b) and 8(c)) of the silicone matrix and TiO_2 -An composites. By plotting the charge density on a log scale, the decay rate of TiO_2 -An yields a straight line,

FIG. 4. The space charge profiles of TiO_2 (left) and ZrO_2 (right) filled silicone at 10 MV/m.

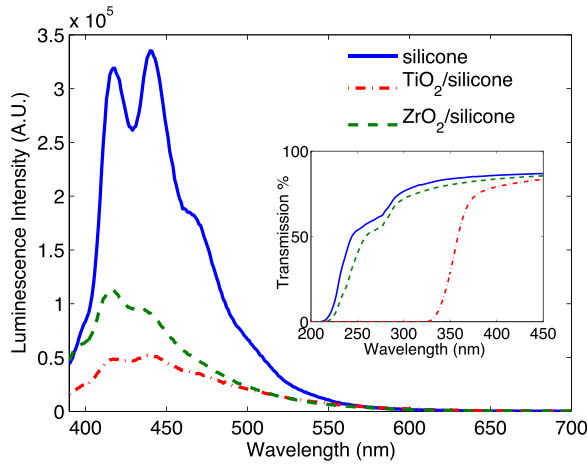


FIG. 5. The emission spectra excited at 370 nm of different samples measured by photoluminescence spectroscopy. The inset graph shows the light transmission spectra measured by UV-Vis spectroscopy.

featuring an exponential decay and a single trap level, in contrast to the downward convex curve of the silicone matrix where the charges are trapped in a distribution of states. By fitting the data, we can estimate the relative trap depth with respect to the energy of the highest occupied states at equilibrium in silicone matrix by $\Delta E = -kT \ln(\tau/\tau_0)$, where τ_0^{-1} is the initial slope of silicone matrix.

The measured space charge profiles of these samples during stressing are plotted in Fig. 9. The calculated EA and IE of different molecules are shown in Table II. The obtained trap depths are summarized in Table III. The electron mobility and trap depth in different composites are essentially the same given that electron trapping predominately occurs on the NP due to its large EA. But there are still some subtle differences. For example, in TiO_2 -AnBr, NBD, and FCHA filled samples, the charge packet traveled a longer distance into the bulk during the transient hopping regime compared to An. The electron transport in AnBr and FCHA filled samples is more dispersive and a few electrons move with longer distance into the bulk at long times. This may relate to the subtle differences in charge trapping kinetics and trap distribution. It is also worth noting that the calculated electron trap depth is only 0.11 eV deeper relative to the traps intrinsically existing in the silicone matrix, even given the large EA of TiO_2 NP. This means that the intrinsic electron traps in bulk silicone are as low as 5 eV below the vacuum level

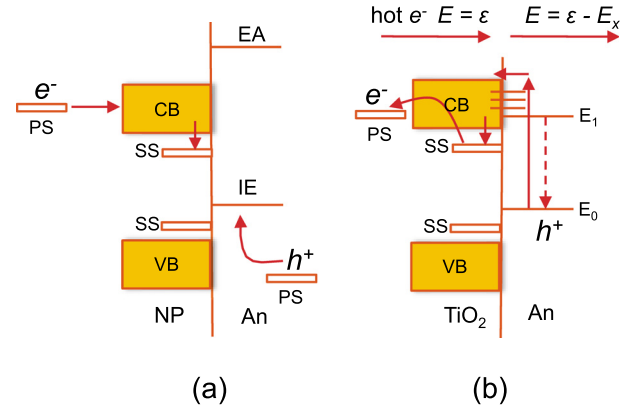


FIG. 7. (a) The illustration of charge trapping at an anthracene grafted TiO_2 nanoparticle. Approximate energy levels are shown. Transferred from the polymer states (PS), electrons are primarily trapped at NPs (possibly at the surface states (SS) while holes are trapped by anthracenes. (b) The illustration of the impact excitation due to hot electrons on anthracene grafted TiO_2 . An electron-hole pair is generated on anthracene, and the excited electron is transferred and then trapped at the surface state of TiO_2 , followed by subsequent detrapping.

(assume vacuum level aligns), which is comparable to the work function of most metals. This is consistent with the large charge transfer rate and thus low energy barrier at the metal/polymer interface observed in space charge measurements³³ and contact electrification experiments.^{34,35}

The hole decay in TiO_2 filled silicones is similar to the fast power-law behavior in the silicone matrix, consistent with the previous observation that TiO_2 does not trap holes (Fig. 4(a)), while the surface states on ZrO_2 increase the hole trap depth by 0.07 eV. The grafted molecules show an increased hole trap depth ranging from 0.07–0.09 eV. This narrow range, however, is not consistent with the large differences in their IE values and the correlation between IE and trap depth is also lacking, as shown in Fig. 10. One possible reason for the discrepancy is that the IE in this case is calculated from an isolated molecule at zero field and does not consider the field effect and electronic interactions with the environment. It has been shown that IE will decrease dramatically with increasing field and the reduction extent varies for different molecules.³⁶ Also, the attachment to NPs and embedding into the polymer may also cause deviations due to possible effects from the electronic interaction and energy alignment with surrounding species.

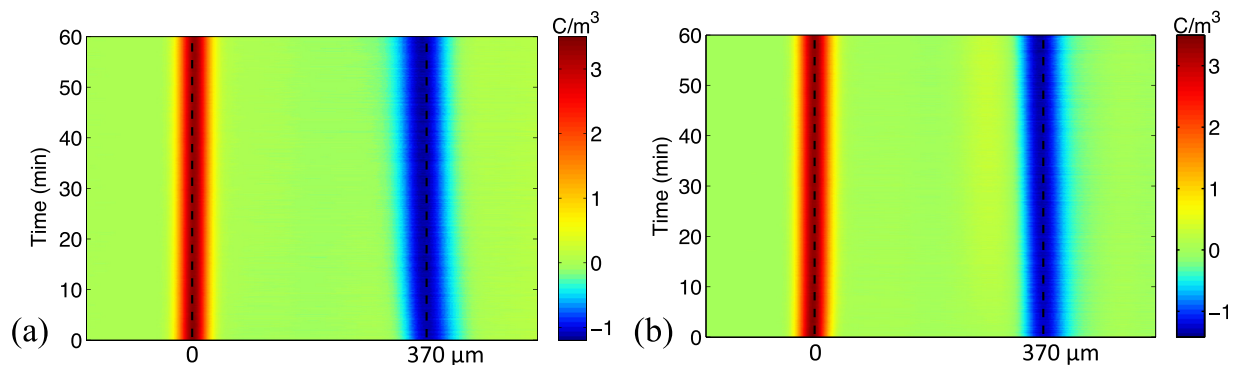


FIG. 6. The space charge profiles of (a) TiO_2 -An and (b) ZrO_2 -An filled silicone at 10 MV/m.

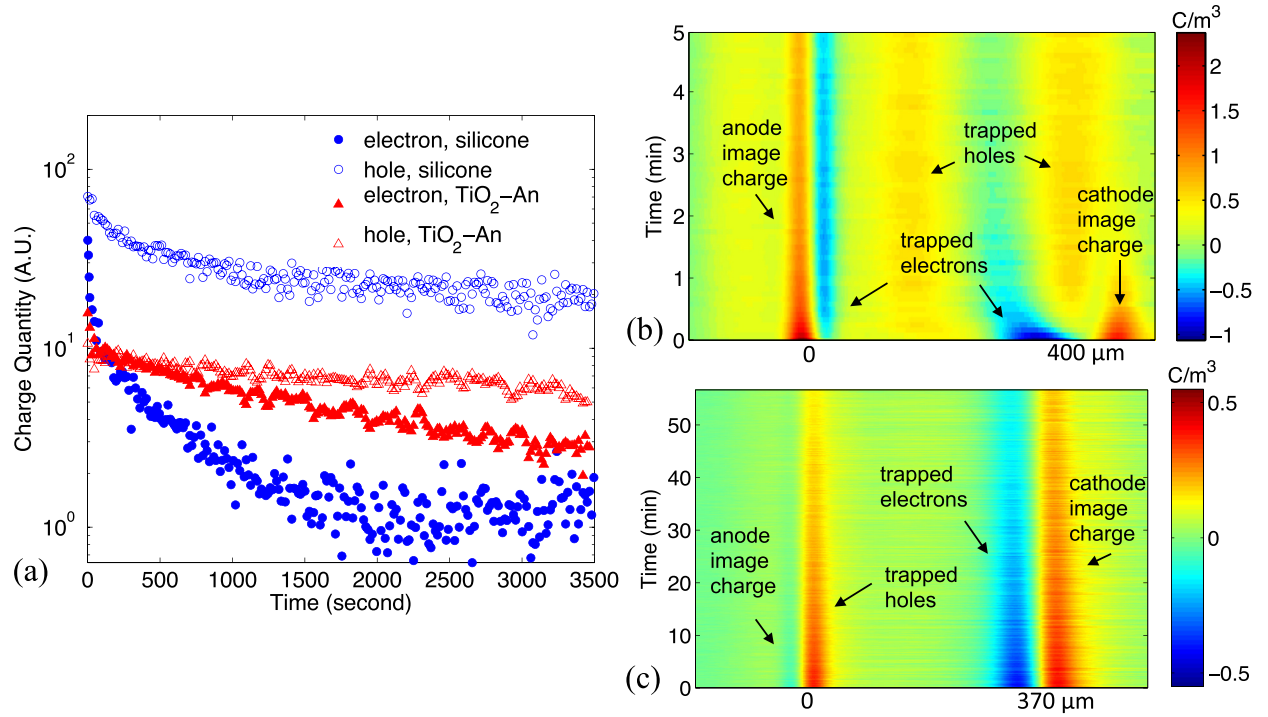


FIG. 8. (a) The plot of remnant charge quantity in silicone matrix and TiO₂-An as a function of time after voltage removal. The electron/hole quantity was obtained by integrating all negative/positive charges in the bulk. The data for silicone matrix is obtained from our previous paper.⁶ (b) The net charge distribution in silicone matrix and (c) in TiO₂-An after stressing at 10 MV/m for 1 h.

The measured DC conductivity and dielectric spectroscopy are plotted in Figs. 11 and 12, respectively, and the results further confirm the trapping effect. At a relatively low field of 10 MV/m, the measured conductivity of TiO₂-An decreased by an order of magnitude compared to the silicone matrix, confirming no percolation of trap sites. The reduced

charge carrier mobility would also decrease the dielectric loss at low frequencies and it was indeed observed in the dielectric spectroscopy. For a better view, the dielectric spectroscopy was plotted in the form of the dielectric susceptibility, which, as suggested by Jonscher, can be defined as $\chi^* = (\epsilon^* - \epsilon_\infty)/\epsilon_0 = \chi' - i\chi''$.³⁷ Here, ϵ_0 is the vacuum

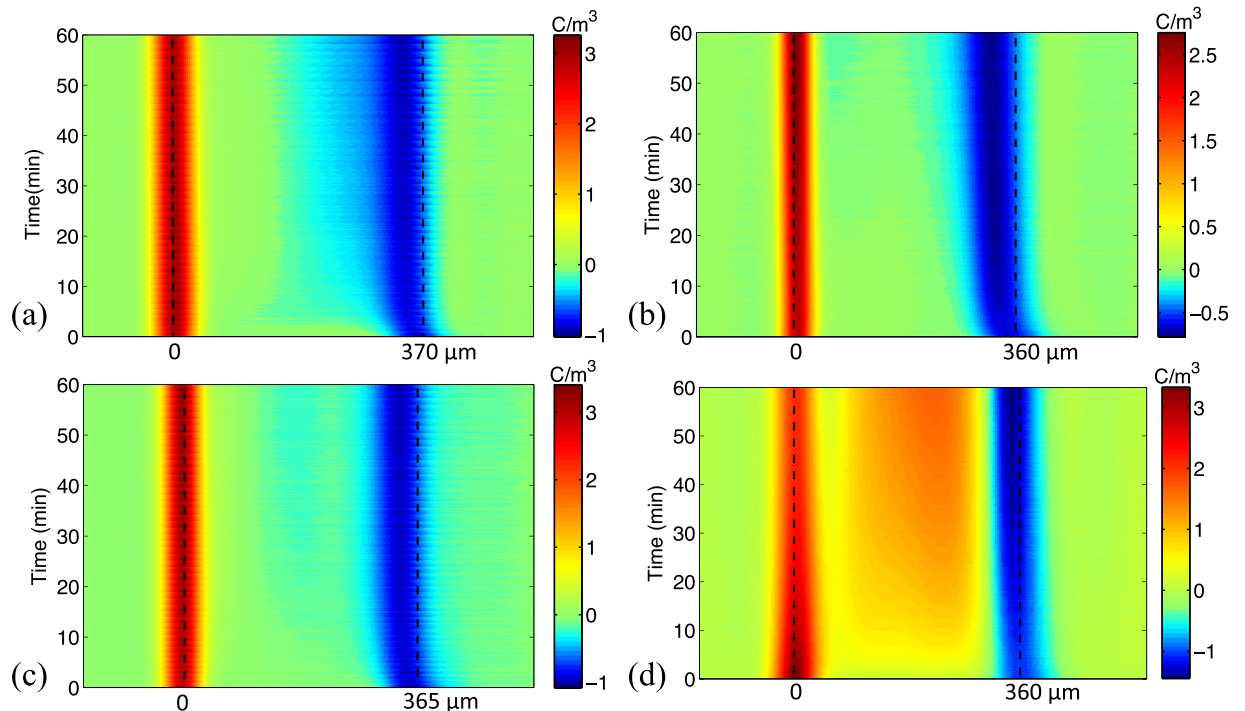


FIG. 9. The space charge profiles of (a) TiO₂-AnBr, (b) TiO₂-NBD, (c) TiO₂-FCHA, and (d) TiO₂-Py at 10 MV/m.

TABLE II. The EA and IE calculated for different small molecules.^a

	An	AnBr	NBD	FCHA	Py
EA (eV)	-1.42	-1.60	-1.89	-1.95	-1.29
-IE (eV)	-7.16	-7.22	-8.34	-5.17	-7.35

^a9-anthracenemethylphosphonic acid (An), 10-bromo-9-methyl anthracene phosphonic acid (AnBr), 3-[N-(7'-Nitrobenz-2'-oxa-1',3'-diazol-4'-yl) amino] propanoic acid (NBD), 6-[Fluorescein-5(6)-carboxamido]hexanoic acid (FCHA), and 1-pyrenecarboxylic acid (Py).

permittivity and ϵ_{∞} is the real permittivity at 1 MHz. The rise of real and imaginary susceptibilities at low frequencies is primarily caused by charge carrier polarization, and it is possible to probe the specific polarization mechanism by analyzing the rising slope. As shown previously,⁶ a transient transport occurs as charges relax into deep states, and the charge carrier mobility as well as the conduction current decreases with time in a power-law fashion as $i = t^{-(1-n)}$, and n is found to increase from zero to close to one at long times. The power-law time dependence exhibits a simultaneous increase of both real and imaginary susceptibilities in the frequency domain as $\chi' \propto \chi'' \propto \omega^{-n}$, which is also known as anomalous low frequency dispersion (LFD) observed in many polymer systems.³⁸ As the silicone matrix is reinforced with a large amount of SiO₂, a strong interfacial polarization will be superimposed on the susceptibility. For interfacial polarization, $\chi'' \propto \omega^{-1}$ and $\chi' \propto \omega^{-2}$.³⁸ This is exactly what we observed in SiO₂ reinforced silicone matrix that $\chi' \propto \omega^{-1.4}$. To exclude the effect of electrode polarization, the dielectric response of the unfilled silicone was also measured, for which the interfacial polarization is absent, thus exhibiting a pure LFD behavior, $\chi' \propto \chi'' \propto \omega^{-0.9}$. Introducing the NP as well as the small conjugated molecules

TABLE III. The comparison of the charge transport parameters for different composites.

Filler	Electron				Hole	
	μ^a (m ² /V s)	L_{\max}^b (μ m)	τ^c ($\times 10^2$ s)	ΔE^d (eV)	τ^c ($\times 10^2$ s)	ΔE^d (eV)
Matrix	2.1×10^{-15}	90	0.38*	0	0.22*	0
TiO ₂	1.5×10^{-16}	12	NA	(-0.11)	0.18*	0
ZrO ₂		23	20	-0.11	33	-0.070
ZrO ₂ -An		7	22	-0.11	83	-0.093
TiO ₂ -An		9	23	-0.11	77	-0.093
TiO ₂ -AnBr		16	11	-0.093	NA	NA
TiO ₂ -NBD		30	22	-0.11	43	-0.077
TiO ₂ -FCHA		14	21	-0.11	40	-0.075
TiO ₂ -Py		12	NA	(-0.11)	31	-0.069

^aThe electron mobility μ is taken from the steady state value.

^b L_{\max} is the total traveling distance of the charge packet within 60 min.

^c τ is fitted the charge decay constant from the exponential decay curve; numbers marked by * indicates a power-law decay curve and the values were obtained by approximating the first 60 s data as an exponential curve; for some samples charges were either mingled with the electrode image charge or shadowed by the opposite charges and could not be analyzed and are noted as NA.

^d ΔE is the increased trap depth compared to the silicone matrix calculated from β , the values in parenthesis are calculated from the steady state electron mobility μ comparing to other samples.

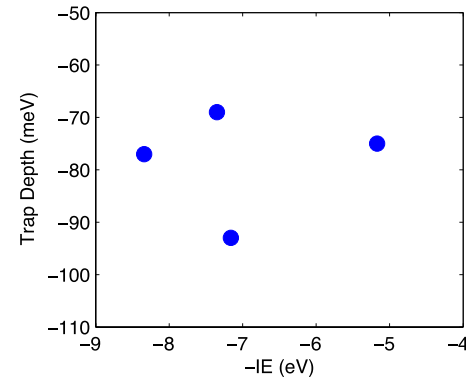


FIG. 10. The correlation between the increased hole trap depth and IE of the small molecules used.

slows down the carrier transport and thus shifts the polarization to lower frequencies, reducing both χ' and χ'' by up to two orders of magnitude. The trend in the extent of reduction is consistent with the space charge and DC conductivity results. Similar reduction in DC conductivity and the dielectric loss at low frequencies has also been found in anthracene grafted SiO₂ filled polypropylene.³⁹

D. Effect on dielectric breakdown and electrical degradation

As shown above, the introduced deep traps can slow down the mobility of space charges and attenuate the field distortion. More importantly, the equilibrium Fermi energy of the injected carriers will be shifted to lower levels in presence of deep traps, which in turn reduces the number of hot carriers that are causing damages to the polymer by breaking bonds and exciting ionizations. As both dielectric breakdown and electrical degradation are impacted by this damage, effective charge trapping is expected to increase the breakdown strength and the lifetime of dielectrics.

To investigate the effect of charge trapping, the time scale of the test must be carefully considered. If the voltage is ramped faster than the thermalization rate of charge carriers, most injected carriers will not be able to reach the deep

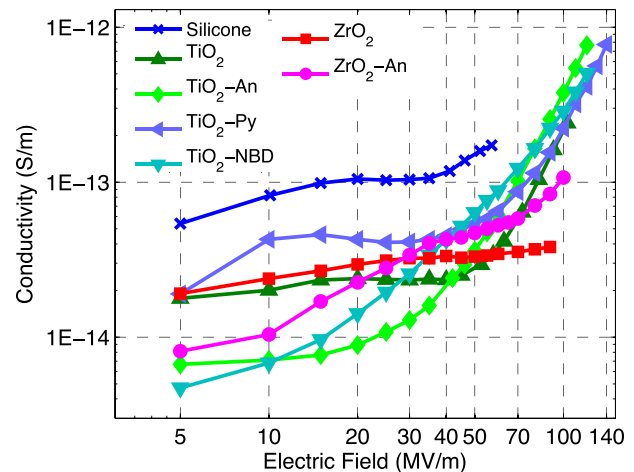


FIG. 11. The measured DC conductivity at an increasing field. The conductivity is obtained using the quasi-steady state current at 10 min after the increase of each voltage step.

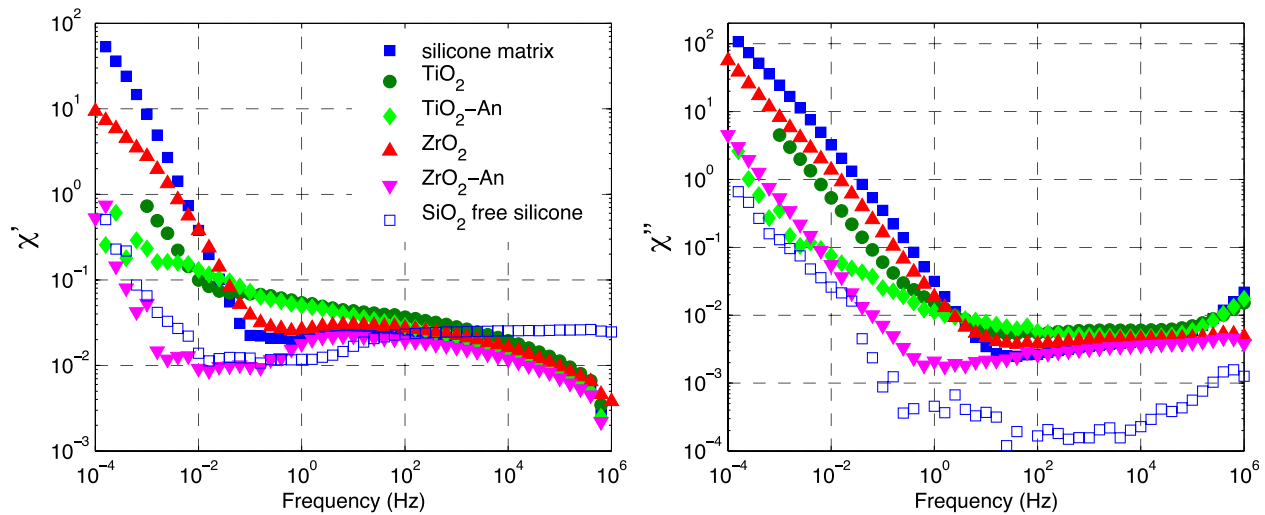


FIG. 12. The real (left) and imaginary (right) dielectric susceptibility of different samples. TiO_2 grafted with other molecules were also measured and show similar response as $\text{TiO}_2\text{-An}$.

traps before breakdown and the breakdown strength will not be largely impacted. Our previous work shows that due to the very low density of deep traps, the equilibration time of charge trapping in silicone can be up to several minutes.⁶ In this case, the NPs are homogeneously dispersed with a concentration comparable to the deep traps intrinsic to silicone, so the equilibration time is not significantly reduced. This is supported by the observed transient electron transport regime at the beginning of the stressing in both filled and unfilled samples. Therefore, a relatively long stressing time was used in the test. The sample was sandwiched between two planar electrodes and was subject to a stepwise field increase of 5 MV/m every 10 min until breakdown. In this fashion, the injected carriers are allowed a relatively long time to relax, so the final breakdown voltage should more faithfully reflect the effect of charge trapping. Three to five samples were measured for each type of composites and the final breakdown field is summarized in Fig. 13. The breakdown field was increased by up to more than 100% for $\text{TiO}_2\text{-An}$ and the trend across systems generally matches that of charge trapping abilities. We also noted that despite having similar charge trapping abilities, TiO_2 filled samples generally exhibit a larger breakdown field compared to ZrO_2 filled ones. The reason will be further discussed in Section IV.

The AC breakdown test results are shown in Fig. 14 and Table IV. Despite the obvious trapping effect, the breakdown strength of ZrO_2 composites is not obviously changed. From previous reasoning, it can be deduced that equilibrium trapping is not reached within the time scale of the AC voltage cycle, and therefore, the breakdown strengths are not largely impacted. But the trapping efficiency and the thermalization rate depend on the trap distribution, and our experiments in polypropylene show that a strong charge trapping from a dense sheet-like SiO_2 NP morphology increases the DC breakdown strength, while reduces the AC breakdown strength possibly by trapped charges enhancing the field distortion near the electrode during polarity switch.³⁹ It is worth noting that small molecule grafted TiO_2 filled samples in this case appear to have a 10% increase in AC breakdown

strength. A similar improvement in AC breakdown strength is also observed in anthracene grafted SiO_2 filled epoxy and polypropylene.^{15,39} This indicates that some other mechanisms besides charge trapping is operating at high field to improve the short-term breakdown strength.

IV. IMPACT EXCITATION AND ITS EFFECT ON DIELECTRIC BREAKDOWN

The high field conduction current data provide a clue to pursue the source of the improvement in AC breakdown strength of TiO_2 composites. As shown in Fig. 11, the composites exhibit lower conductivity at low field due to the charge trapping effect and the trend is consistent with the PEA results. The conductivities increase slowly with field, except for the TiO_2 filled samples showing a super-linear increase of conductivity at higher fields. Since TiO_2 and ZrO_2 have a similar trap depth, we would expect the charge mobility in TiO_2 filled samples to follow the same trend as ZrO_2 . Therefore, this anomalous increase of conductivity is likely to be caused by an increase in charge carrier density. To verify this, we measured the charge density in $\text{TiO}_2\text{-An}$ at an increasing field up to 45 MV/m using PEA, and it was found

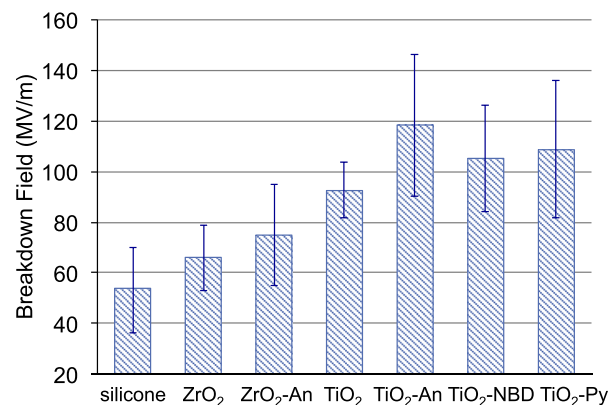


FIG. 13. Final breakdown field of the sample in the DC conductivity measurement. The value is averaged over several samples, and the error bar marks the highest and lowest value obtained.

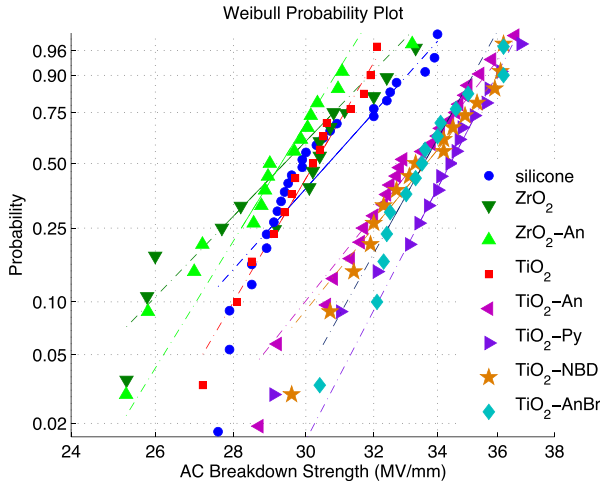


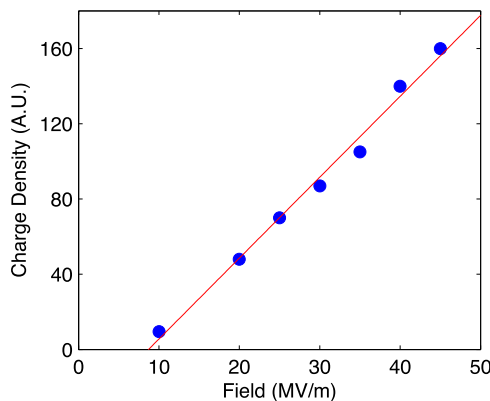
FIG. 14. The Weibull plot of AC breakdown strength.

TABLE IV. The AC dielectric breakdown strength (DBS).

Sample	AC DBS (MV/m)	Relative change (%)	Weibull shape parameter
Silicone	31.2	0	16.5
ZrO ₂	30.6	-2	14.7
ZrO ₂ -An	30.0	-4	16.3
TiO ₂	30.6	-2	25.3
TiO ₂ -An	33.9	9	19.7
TiO ₂ -AnBr	34.3	10	23.3
TiO ₂ -NBD	34.3	10	20.5
TiO ₂ -Py	34.5	11	24.2

that the net space charge density in the bulk of the sample still maintained a linear relationship with field (Fig. 15). A possible explanation is that the additional charge carriers were generated in the bulk by ionization of the neutral species so the net charge density did not change.

We note that TiO₂ NP and grafted organic molecules have rather smaller excitation energies of 3 to 4 eV so that they are easier to excite by hot carriers than silicone. It can be speculated that the super-linear increase of current in these samples is caused by bulk generated charge carriers from the impact excitation of TiO₂ NP and grafted organic

FIG. 15. The total net charge density (negative) in the bulk of TiO₂-An sample as a function of field after 10 min stressing.

molecules. Also, the breakdown field of silicone is only 30 MV/m under AC and 50 MV/m under DC conditions, which means that in this field range, some carriers can already be accelerated to sufficient energies to cause damages to the polymer. Given the greater excitation energy of silicone polymer, it is not unreasonable to expect impact excitations on TiO₂ and grafted molecules in the measured field range. Though difficult to detect in a solid, the phenomenon of impact excitation or ionization on small excitation energy or low IE molecules is more visible in liquid.^{40,41} For instance, when the low IE pyrene (IE = 7.5 eV) was introduced to cyclohexane (IE = 9.9 eV), the easy ionization of pyrene significantly reduced the streamer inception voltage and induced a much more branched streamer geometry.⁴⁰ In the solid, the created ions are less mobile and cannot form streamers. On the other hand, the impact excitation can be beneficial for retarding the electrical aging and dielectric breakdown because it effectively dissipates the energy of hot carriers in the form of heat and light and thus minimizes the direct damages to the polymer. This effect was suggested to be responsible for the retarded first mode negative streamer growth, reduced negative charge injection, and increased light emission in *N,N*-dimethylaniline filled *n*-tridecane.^{42,43} Based on the reasoning above, the improved breakdown strength for TiO₂ filled samples is likely caused by this impact excitation effect.

Impact excitation rather than ionization is considered to be the dominant process in this case. Excitation requires a much smaller energy threshold than direct ionization. In contrast to crystalline materials, polymers are mostly disordered, and the excited charge carriers are not readily available for band transport but confined to localized states. It was suggested that these created localized excitons can recombine or later be separated by field and contribute to the current by a two-step ionization process.³⁶ This is supported by our experiment results as well as other evidences from the literature.

The first piece of evidence comes from the DC conductivity data. Despite the same IE for ZrO₂ and TiO₂, only TiO₂ filled samples showed a super-linear current increase. This can be readily explained in terms of impact excitation because ZrO₂ has a much larger band gap of 5.8 eV and is less likely to be excited in the given field range. Another piece of evidence is obtained from the current profiles of different molecules grafted TiO₂. Fig. 16 plots the onset electric field of the super-linear current with the excitation energy and IE of TiO₂ NP and different molecules, respectively. The excitation energy was obtained from the maximum light absorption wavelength in UV-Vis spectroscopy. It was found that the excitation energy gives a better correlation with the onset field than IE. The onset field decreases monotonically with decreasing excitation energy in an almost linear fashion. This is as expected because the energy of hot carriers should increase with field and only carriers with sufficient energies can cause impact excitation. These observations support the hypothesis that rather by directly ionizing the molecule or NP, hot carriers would first create excitons on these species, which then either recombine directly or separate by field.

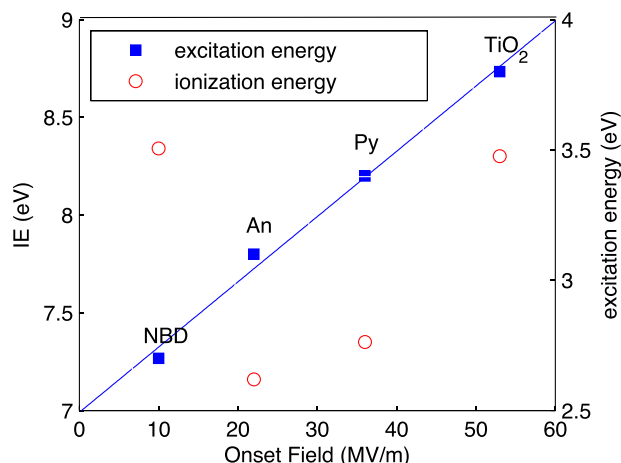


FIG. 16. The onset field of the super-linear current increase as a function of IE and excitation energy, respectively.

The detailed process of impact excitation is illustrated in Fig. 7(b). If the excitation happens on the TiO_2 NP, the excited charges may become trapped at a surface state, which retards the recombination process and allows more time for charges to detrapp and contribute to the current. Time resolved photoluminescence spectroscopy revealed that if the excitation occurs at the anthracene molecule, the excited electron is likely to transfer to TiO_2 and be trapped there.⁴⁴ This is because the lowest unoccupied molecular orbital (LUMO) (which is not equal to EA as the LUMO here is calculated from a charge neutral molecule) of anthracene lies within the conduction band of TiO_2 so that the transfer is favorable. ZrO_2 NPs have a much larger band gap ~ 5.8 eV and are not likely to be excited in the given field range, so no large increase in conductivity is observed. For ZrO_2 -An, the excitation can happen at anthracene, but the interfacial electron transfer is rather limited because the LUMO of anthracene lies below the CBM of ZrO_2 .^{30,44} Thus, the exciton on anthracene is more likely to relax by direct recombination and will not contribute significantly to the conduction. We measured the photoluminescence of ZrO_2 -An and TiO_2 -An filled silicone at the anthracene excitation wavelength of 370 nm, and the intensity of the former is found to be nearly two orders of magnitude greater than the latter, manifesting a much higher probability for radiative recombination (see Fig. S3 in the supplementary material²⁹). This explains why the conductivity of ZrO_2 -An filled samples increases much more slowly compared to TiO_2 -An, given that most excitons went through recombination rather than separation. The recombination should result in a characteristic emission band from the small molecule. Yamono and Iizuka measured the electroluminescence spectra of anthracene doped low-density polyethylene (LDPE) and found that compared to neat LDPE, there was an additional peak around 400 nm, which falls into the luminescence range of anthracene,² which further supports a subsequent radiative recombination after excitation.

The excited charges will not contribute to current unless they leave the molecule or NP. The detrapping process from neutral species can be described using the Poole-Frenkel model⁴⁵ in which the maximum barrier decreases with field as $\Delta E = \Delta E_0 - \frac{e^{3/2} F^{1/2}}{(4\pi\epsilon_0\epsilon_r)^{1/2} k_B T}$. If the increase in conductivity is

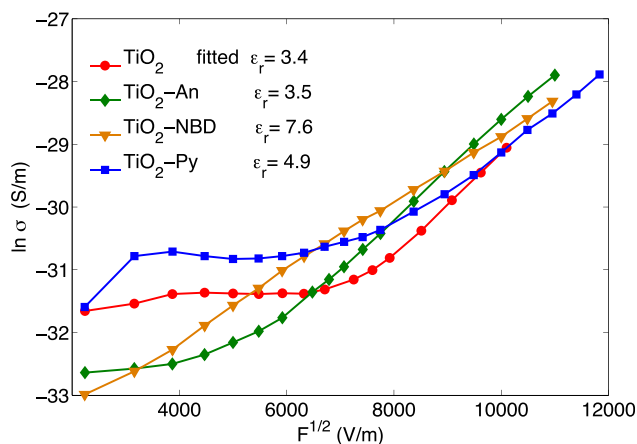


FIG. 17. The log of conductivity versus the square root of field of different TiO_2 filled samples.

limited by the detrapping process and as $\sigma \propto \exp(-E/k_B T)$, plotting $\ln \sigma$ with $F^{1/2}$ should yield a linear line. The results for some TiO_2 based composites are plotted in Fig. 17, and the high field part shows a fairly good linearity. The different fitted slope reflects the local permittivity at the interfacial region, and the values were calculated, as shown in Fig. 17. These values are in a reasonable agreement with what we expected for silicone, and the polar molecule NBD yields a higher local permittivity at the interface.

V. CONCLUSION

By specifically controlling the dispersion of nanoparticles and organic additives in polymers, it is allowed to more legitimately examine their electronic effects on charge transport and dielectric breakdown of polymers. Two effects of the added species were identified in this investigation of silicone nanodielectrics: charge trapping and impact excitation, and both contribute to an enhancement of the breakdown strength.

Electrons are trapped in ZrO_2 and TiO_2 NPs while holes are primarily trapped at the grafted molecules, which can be qualitatively explained by their drastically different ionization energies and electron affinities. But a quantitative correlation between the measured trap depth and computed ionization energy still remain elusive. The deviation may be attributed to the field effect and electronic interactions with the surrounding environment, which can impact electronic energies but are not specifically considered in this DFT modeling. Nevertheless, the effective trapping from these fillers was found to reduce the conductivity and field distortion, and the breakdown strength was most significantly increased when the stressing time is longer than the equilibration time of trapping. The charge trapping from organic molecules grafted NP is not unique for silicone and is also evidenced in our studies in epoxy and polypropylene systems.^{4,15,39} However, the measured “effective” trap depth from the extrinsic species is much smaller than predicted by treating the polymer as a perfect crystal free of traps. This large discrepancy is attributed to the intrinsic traps originally present in polymers extending deep into the energy gap, which reduce the effect of these new traps. Though pursued for a long time by scientists, the nature of these

intrinsic trap states is still not well understood. Theories of morphological defects,⁴⁶ chemical impurities,^{47,48} and traps due to induced energy relaxation of polymers³⁴ have been proposed, but the studies are still far from satisfactory. This uncertainty, undoubtedly brings more difficulties for material design to predict the trap depth and charge mobility by *ab initio* modeling, and further efforts in this field are still encouraged.

It was also postulated that the impact excitation is another important mechanism that can lead to retarded degradation and increased breakdown strength. The hot carriers with enough energy can excite an electron-hole pair on the introduced low excitation energy species upon collision, with the energy of itself effectively dissipated. This hypothesis can reasonably explain the increased breakdown strength of TiO₂ filled samples, and is supported by the *I*-*V* behavior and photoluminescence of the composites, as well as the electroluminescence evidences in both liquid and solid dielectrics from previous literature. More substantiate evidence may be found by electroluminescence measurement for this particular case and remains to be further explored.

ACKNOWLEDGMENTS

The authors wish to acknowledge the financial support from the Office of Naval Research (N000141310173) and express thanks to Professor Keith Nelson and Professor Toh-Ming Lu from Rensselaer Polytechnic Institute, and Dr. Mikael Unge and Dr. Joakim Jambeck from ABB corporate research center in Sweden for many useful discussions.

- ¹T. Tanaka, *IEEE Trans. Dielectr. Electr. Insul.* **12**, 914–928 (2005).
- ²Y. Yamano and M. Iizuka, *IEEE Trans. Dielectr. Electr. Insul.* **16**, 189–198 (2009).
- ³V. Englund, R. Huuva, S. M. Gubanski, and T. Hjertberg, *Polym. Degrad. Stab.* **94**, 823–833 (2009).
- ⁴S. Virtanen, T. M. Krentz, J. K. Nelson, L. S. Schadler, M. Bell, B. Benicewicz, H. Hillborg, and S. Zhao, *IEEE Trans. Dielectr. Electr. Insul.* **21**, 563–570 (2014).
- ⁵R. C. Smith, Ph.D. thesis, Rensselaer Polytechnic Institute, 2009.
- ⁶Y. Huang and L. S. Schadler, *J. Appl. Phys.* **120**, 055101 (2016).
- ⁷C. Calebrese, L. Hui, L. S. Schadler, and J. K. Nelson, *IEEE Trans. Dielectr. Electr. Insul.* **18**, 938–945 (2011).
- ⁸B. Natarajan, Y. Li, H. Deng, L. C. Brinson, and L. S. Schadler, *Macromolecules* **46**, 2833–2841 (2013).
- ⁹Y. Li, P. Tao, A. Viswanath, B. C. Benicewicz, and L. S. Schadler, *Langmuir* **29**, 1211–1220 (2013).
- ¹⁰Y. Li, L. Wang, B. Natarajan, P. Tao, B. C. Benicewicz, C. Ullal, and L. S. Schadler, *RSC Adv.* **5**, 14788–14795 (2015).
- ¹¹Y. Li, T. M. Krentz, L. Wang, B. C. Benicewicz, and L. S. Schadler, *ACS Appl. Mater. Interfaces* **6**, 6005–6021 (2014).
- ¹²Y. Qiao, X. Yin, L. Wang, M. S. Islam, B. C. Benicewicz, H. J. Ploehn, and C. Tang, *Macromolecules* **48**, 8998–9006 (2015).
- ¹³Y. Huang, T. M. Krentz, J. K. Nelson, L. S. Schadler, M. Bell, and B. Benicewicz, “Bimodal brush functionalized TiO₂/silicone nanocomposites with improved dielectric properties,” in *Proceedings of Electrical Insulation Conference, Seattle, USA* (IEEE, 2015), p. 325–328.
- ¹⁴Y. Li, Ph.D. thesis, Rensselaer Polytechnic Institute, 2014.
- ¹⁵T. M. Krentz, Y. Huang, J. K. Nelson, L. S. Schadler, M. Bell, B. Benicewicz, S. Zhao, and H. Hillborg, “Enhanced charge trapping in bimodal brush functionalized silica-epoxy nanocomposite dielectrics,” in *Proceedings of Electrical Insulation and Dielectric Phenomena (CEIDP), Des Moines, USA* (IEEE, 2014), pp. 643–646.
- ¹⁶M. J. Frisch, G. W. Trucks, H. B. Schlegel, G. E. Scuseria, M. A. Robb, J. R. Cheeseman, G. Scalmani, V. Barone, B. Mennucci, G. A. Petersson, H. Nakatsuji, M. Caricato, X. Li, H. P. Hratchian, A. F. Izmaylov, J. Bloino, G. Zheng, J. L. Sonnenberg, M. Hada, M. Ehara, K. Toyota, R. Fukuda, J. Hasegawa, M. Ishida, T. Nakajima, Y. Honda, O. Kitao, H. Nakai, T. Vreven, J. A. Montgomery, Jr., J. E. Peralta, F. Ogliaro, M. J. Bearpark, J. Heyd, E. N. Brothers, K. N. Kudin, V. N. Staroverov, R. Kobayashi, J. Normand, K. Raghavachari, A. P. Rendell, J. C. Burant, S. S. Iyengar, J. Tomasi, M. Cossi, N. Rega, N. J. Millam, M. Klene, J. E. Knox, J. B. Cross, V. Bakken, C. Adamo, J. Jaramillo, R. Gomperts, R. E. Stratmann, O. Yazyev, A. J. Austin, R. Cammi, C. Pomelli, J. W. Ochterski, R. L. Martin, K. Morokuma, V. G. Zakrzewski, G. A. Voth, P. Salvador, J. J. Dannenberg, S. Dapprich, A. D. Daniels, Ö. Farkas, J. B. Foresman, J. V. Ortiz, J. Cioslowski, and D. J. Fox, *Gaussian 09* (Gaussian, Inc., Wallingford, CT, USA, 2009).
- ¹⁷C. Lee, W. Yang, and R. G. Parr, *Phys. Rev. B* **37**, 785 (1988).
- ¹⁸B. Miehllich, A. Savin, H. Stoll, and H. Preuss, *Chem. Phys. Lett.* **157**, 200–206 (1989).
- ¹⁹A. D. Becke, *J. Chem. Phys.* **98**, 5648–5652 (1993).
- ²⁰W. R. Duncan and O. V. Prezhdo, *Ann. Rev. Phys. Chem.* **58**, 143–184 (2007).
- ²¹H. Zhang, Y. Shang, X. Wang, H. Zhao, B. Han, and Z. Li, *J. Mol. Model.* **19**, 5429–5438 (2013).
- ²²Y. Yamano, *IEEE Trans. Dielectr. Electr. Insul.* **13**, 773–781 (2006).
- ²³Y.-C. Yeo, T.-J. King, and C. Hu, *J. Appl. Phys.* **92**, 7266–7271 (2002).
- ²⁴H. Vázquez, Y. Dappe, J. Ortega, and F. Flores, *J. Chem. Phys.* **126**, 144703 (2007).
- ²⁵H. Ishii, K. Sugiyama, E. Ito, and K. Seki, *Adv. Mater.* **11**, 605–625 (1999).
- ²⁶A. Köhler and H. Bässler, *Electronic Processes in Organic Semiconductors: An Introduction* (John Wiley & Sons, 2015).
- ²⁷V. Kasperovich, K. Wong, G. Tikhonov, and V. V. Kresin, *Phys. Rev. Lett.* **85**, 2729–2732 (2000).
- ²⁸A. Rungta, B. Natarajan, T. Neely, D. Dukes, L. S. Schadler, and B. C. Benicewicz, *Macromolecules* **45**, 9303–9311 (2012).
- ²⁹See supplementary material at <http://dx.doi.org/10.1063/1.4959771> for more information.
- ³⁰G. Ramakrishna, A. K. Singh, D. K. Palit, and H. N. Ghosh, *J. Phys. Chem. B* **108**, 4775–4783 (2004).
- ³¹D. O. Scanlon, C. W. Dunnill, J. Buckridge, S. A. Shevlin, A. J. Logsdail, S. M. Woodley, C. R. A. Catlow, M. J. Powell, R. G. Palgrave, and I. P. Parkin, *Nat. Mater.* **12**, 798–801 (2013).
- ³²J. Robertson, *J. Vac. Sci. Technol. B* **18**, 1785–1791 (2000).
- ³³K. Matsui, Y. Tanaka, T. Takada, T. Fukao, K. Fukunaga, T. Maeno, and J. M. Alison, *IEEE Trans. Dielectr. Electr. Insul.* **12**, 406–415 (2005).
- ³⁴C. Duke and T. Fabish, *Phys. Rev. Lett.* **37**, 1075 (1976).
- ³⁵T. Fabish, H. Saltsburg, and M. Hair, *J. Appl. Phys.* **47**, 930–939 (1976).
- ³⁶N. Davari, P.-O. Åstrand, S. Ingebrigtsen, and M. Unge, *J. Appl. Phys.* **113**, 143707 (2013).
- ³⁷A. K. Jonscher, *Nature* **267**, 673–679 (1977).
- ³⁸A. Jonscher, *Philos. Mag. B* **38**, 587–601 (1978).
- ³⁹T. Krentz, M. M. Khani, M. Bell, B. C. Benicewicz, J. K. Nelson, S. Zhao, H. Hillborg, and L. S. Schadler, “Morphologically dependent AC and DC breakdown strength in silica-polypropylene nanocomposites,” *J. Appl. Polym. Sci.* (submitted).
- ⁴⁰O. Lesaint and M. Jung, *J. Phys. D: Appl. Phys.* **33**, 1360 (2000).
- ⁴¹M. Unge, S. Singha, S. Ingebrigtsen, D. Linhjell, and L. Lundgaard, “Influence of molecular additives on positive streamer propagation in ester liquids,” in *Proceedings of 18th International Conference on Dielectric Liquids (ICDL), Bled, Slovenia* (IEEE, 2014), pp. 1–4.
- ⁴²Ø. L. Hestad, H. Smalø, P.-O. Åstrand, S. Ingebrigtsen, and L. Lundgaard, *IEEE Trans. Dielectr. Electr. Insul.* **18**, 1886–1896 (2011).
- ⁴³H. S. Smalø, Ø. Hestad, S. Ingebrigtsen, and P.-O. Åstrand, *J. Appl. Phys.* **109**, 073306 (2011).
- ⁴⁴I. Martini, J. H. Hodak, and G. V. Hartland, *J. Phys. Chem. B* **102**, 9508–9517 (1998).
- ⁴⁵L. A. Dissado and J. C. Fothergill, *Electrical Degradation and Breakdown in Polymers* (IET, 1992).
- ⁴⁶Y. Wang, D. MacKernan, D. Cubero, D. F. Coker, and N. Quirke, *J. Chem. Phys.* **140**, 154902 (2014).
- ⁴⁷G. Teyssedre and C. Laurent, *IEEE Trans. Dielectr. Electr. Insul.* **12**, 857–875 (2005).
- ⁴⁸L. Chen, T. D. Huan, A. Huzayyin, Y. C. Quintero, and R. Ramprasad, “First-principles study of aluminum-polyethylene interfaces,” in *Proceedings of Electrical Insulation and Dielectric Phenomena (CEIDP), Des Moines, USA* (IEEE, 2014), pp. 887–890.